Journal of Power Sources 196 (2011) 7104–7109

Contents lists available at ScienceDirect

Journal of Power Sources

journal homepage: www.elsevier.com/locate/jpowsour

Solid oxide fuel cell composite cathodes based on perovskite and fluorite structures

Vladislav Sadykov[a,b,*], Natalia Mezentseva[a], Vladimir Usoltsev[a], Ekaterina Sadovskaya[a], Arkady Ishchenko[a], Svetlana Pavlova[a], Yulia Bespalko[a], Tamara Kharlamova[a], Ekaterina Zevak[a,b], Aleksei Salanov[a], Tamara Krieger[a], Vladimir Belyaev[a], Oleg Bobrenok[c], Nikolai Uvarov[d], Yury Okhlupin[d], Oleg Smorygo[e], Alevtina Smirnova[f], Prabhakar Singh[g], Aleksandr Vlasov[h], Mikhail Korobeynikov[h], Aleksandr Bryazgin[h], Peter Kalinin[h], Andrei Arzhannikov[h]

[a] *Boreskov Institute of Catalysis SB RAS, Novosibirsk, 630090, Russian Federation*
[b] *Novosibirsk State University, Novosibirsk, 630090, Russian Federation*
[c] *Institute of Thermal Physics SB RAS, Novosibirsk, 630090, Russian Federation*
[d] *Institute of Solid State Chemistry and Mechanical Activation, Novosibirsk, 630090, Russian Federation*
[e] *Powder Metallurgy Institute, Minsk, Belarus*
[f] *Eastern Connecticut State University, Willimantic, CT, USA*
[g] *University of Connecticut, Storrs, CT, USA*
[h] *Budker Institute of Nuclear Physics, Novosibirsk, 630090, Russian Federation*

ARTICLE INFO

Article history:
Received 24 June 2010
Accepted 28 July 2010
Available online 18 August 2010

Keywords:
SOFC
Cathode nanocomposites
Ultrasonic treatment
Radiation–thermal sintering
Oxygen mobility
Cell performance

ABSTRACT

This work presents the results related to the functionally graded fluorite (F)–perovskite (P) nanocomposite cathodes for IT SOFC. Nanocrystalline fluorites (GDC, ScCeSZ) and perovskites (LSrMn, LSrFNi) were synthesized by Pechini method. Nanocomposites were prepared by the ultrasonic dispersion of F and P powders in isopropanol with addition of polyvinyl butyral. Different techniques for deposition and sintering of functionally graded cathode materials were applied including traditional approaches as well as original methods, such as radiation–thermal sintering under electron beam or microwave radiation. Morphology, microstructure and elemental composition of nanocomposites was characterized by XRD and HRTEM/SEM with EDX. Even for dense composites, the sizes of perovskite and fluorite domains remain in the nanorange providing developed P–F interfaces. Oxygen isotope heteroexchange and conductivity/weight relaxation studies demonstrated that these interfaces provide a path for fast oxygen diffusion. The redistribution of the elements between P and F phases in nanocomposites occurs without formation of insulating zirconate phases. Button-size fuel cells with nanocomposite functionally graded cathodes, thin YSZ layers and anode Ni/YSZ cermet (either bulk or supported on Ni–Al foam substrates) were manufactured. For optimized composition and functionally graded design of P–F nanocomposite cathodes, a stable performance in the intermediate temperature range with maximum power density up to 0.5 W cm^{-2} at 700 °C in wet H_2/air feeds was demonstrated.

1. Introduction

One of the most important task in solid oxide fuel cell research is to decrease their operation temperature to 600–800 °C. This can be achieved by application of cathode materials possessing high mixed ionic–electronic conductivity and chemically compatible with YSZ [1–5]. Moreover, this approach allows improving cell performance and endurance due to decrease of the interface resistance, increase of triple-phase boundaries and CTE matching. Composites comprised of GDC, YSZ (ScCeSZ) and Sr-doped complex perovskites (LSM, LSFC, LSFN) are suggested for design of functionally graded cathodes [1–9]. To provide high and stable performance of SOFC with these materials, optimization of their composition, synthesis procedure and microstructure as well as methods of supporting and sintering of functionally graded cathode layers is required which is the aim of present research.

Since perovskite–fluorite interfaces in composite materials appear to be important for fast oxygen diffusion [6–10], the main approach used in this work was based upon application of synthesis procedures potentially able to ensure spatially uniform distribution

* Corresponding author at: Boreskov Institute of Catalysis, Pr. Lavrentieva, 5, 630090 Novosibirsk, Russian Federation. Tel.: +7 383 330 8763; fax: +7 383 330 8056.
E-mail addresses: sadykov@catalysis.ru, sadykovy@academ.org (V. Sadykov).

0378-7753/$ – see front matter © 2010 Elsevier B.V. All rights reserved.
doi:10.1016/j.jpowsour.2010.07.096

of particles of constituting phases in nanocomposites and their sizes remaining in nanorange even in dense materials. Hence, nanocrystalline perovskites and fluorites as starting materials, a powerful ultrasonic treatment in organic solvents and new techniques of composite layers sintering at decreased temperatures under action of electron beam or microwave radiation as well as sintering aids were applied. Microstructural features of composites were systematically compared with their transport properties characterized both for dispersed and dense samples using a unique combination of methods. Performance of nanocomposites possessing the most attractive properties was verified by their testing as functionally graded cathodes in button-size fuel cells with thin YSZ layers.

2. Experimental

$La_{0.8}Sr_{0.2}Fe_{1-x}Ni_xO_{3-\delta}$ ($x = 0.1$–0.4) ($LSFN_x$) and $La_{0.8}Sr_{0.2}MnO_{3+x}$ (LSM) perovskites and $Ce_{0.9}Gd_{0.1}O_{2-\delta}$ (GDC) fluorite were synthesized by Pechini route using metal nitrates, citric acid, ethylene glycol and ethylenediamine as reagents [10]. Commercial sample of ScCeSZ (DKKK corporation, Japan) and samples of GDC, LSM and LSNF synthesized via Pechini route and calcined at 500 (GDC) or 700 °C (perovskites) were used for nanocomposites preparation via ultrasonic dispersion of the mixture of powders in isopropanol using a T25 ULTRA-TURRAX (IKA, Germany) homogenizer with addition of polyvinyl butyral followed by drying, pressing pellets and their sintering in air up to 1300 °C.

XRD patterns were obtained with an ARLX'TRA diffractometer (Thermo, Switzerland) using Cu K_α monochromatic radiation ($\lambda = 1.5418$ Å) in 2θ in the range 5–90°.

Transmission Electron Microscopy (TEM) micrographs were obtained with a JEM-2010 instrument (lattice resolution 1.4 Å, acceleration voltage 200 kV). Analysis of the local elemental composition was carried out by using an energy-dispersive EDX spectrometer equipped with Si(Li) detector (energy resolution 130 eV).

Morphology of the surface layer of sintered nanocomposite pellets and cathode layers was studied by SEM using a JSM-6460 LV (Jeol) microscope with EDX Phoenix Spectrometer.

The rate of the surface reaction of oxygen molecules activation and oxygen mobility of LSFN + GDC composite were characterized by the oxygen isotope heteroexchange in a flow installation (SSITKA mode [11]) with MS control of the gas phase isotope composition. The data analysis with a due regard for the mechanism of oxygen isotope exchange, surface reaction and bulk diffusion was carried out by the inverse problem solution for the system of hyperbolic differential equations describing the isotope exchange in the flow reactor following earlier published approaches [11].

Electrical conductivities of cathode materials and relaxation profiles were measured using the four-probe Van der Pauw method with platinum wires as current and voltage electrodes. The measuring cell included $Zr(Y)O_2$ test tube with the electrochemical oxygen pump. Instrument/device control and data acquisition used LabVIEW (National Instruments). For the abrupt change in oxygen pressure at the beginning of the reducing/oxidation step the sample inside the electrochemical pump was blown by a pulse of the helium/oxygen flow with a maximal rate of 200 mL min^{-1}. Then the pressure was regulated by the PID-regulator of the electrochemical oxygen pump with an accuracy of $\Delta P = 10^{-5}$ bar. The holder accommodates a sample with the maximum length of the side of a square sample of 0.5 cm and holds all four platinum electrodes and a K-type thermocouple. The diameter of contact of the sample and the probe did not exceed 0.3 mm. Estimation of chemical oxygen diffusion coefficient D_{chem} and surface exchange constant k_{chem} by analysis of conductivity transients after changing the oxygen partial pressure was carried out using the model of diffusion in a thin infinite plate following earlier described approaches [12–14].

For dense LSFN perovskite and LSFN + GDC nanocomposite pellets, the oxygen chemical diffusion coefficients and amount of easily removed oxygen were estimated by analysis of their weight relaxation [15] after step-wise change of O_2 content in the N_2 stream from 14 to 1.4% using a STA 409 PC "LUXX" NETZSCH machine.

For assembling cells, a home-made Ni/YSZ anode substrate (either bulk cermet [7,8] or cermet layers supported onto compressed foam Ni–Al alloy substrate ([16]) with 10 μm thick 8YSZ layers supported by CVD were used. Cathode slurries made from nano-powders ultrasonically dispersed in isopropanol with addition of butyral resin were deposited on half cells by the air spray (GDC or perovskite + fluorite 10 μm thick nanocomposite functional layer) and by painting (porous thick LSFN or LSM cathode layer). Functional interlayers were sintered either in the furnace at temperatures up to 1200 °C (nanocomposites) or 1400 °C (GDC) with or without sintering aids (Bi or Ag nitrates), or under the action of microwave radiation (5 kW, 24 GHz microwave oven)/electron beam (electron energy 2.4 MeV, pulses frequency varied from 1 to 25 Hz).

For SOFC testing, the planar cell 2 cm × 2 cm was put between the polished end faces of two corundum tubes (internal diameter 1 cm) and compressed by springs thus providing gas chambers for supply of air as oxidant (200 mL min^{-1}) and wet hydrogen as fuel (100 mL min^{-1}). Pt meshes along with Ag paste were used as the current collectors. After anode reduction by H_2 at 700 °C for several hours, the *I–V* curves were measured at 600–800 °C.

The cells after testing were studied by SEM with EDX analysis. To prepare the cross-section, the sample was fixed in epoxide resin and the cell chip was polished using Cr_2O_3 as a brightener.

3. Results and discussion

3.1. Structural and microstructural characterization of nanocomposite materials

In all composites sintered at temperatures below 1200 °C, only phases corresponding to initial perovskite (P) and fluorite-like (F) phases were observed [6–10]. The shift of diffraction peaks with sintering temperature revealed redistribution of cations between P and F phases, which was confirmed by HRTEM with EDX analysis (Fig. 1). The most general feature observed by EDX and X-ray Photoelectron Spectroscopy [6,10] for all nanocomposite systems is a partial transfer of La, Sr and transition metal cations into the surface layers of fluorite-like oxides forming surface phases of a perovskite type (cerates, zirconates) with mixed ionic–electronic conductivity. This provides a good epitaxy between perovskite and fluorite domains which remain in the nanorange (<100 nm as estimated by XRD and TEM data) even in dense materials. Moreover, these domains are arranged into bigger crystallites with well-defined faces densely packed in sintered nanocomposites thus providing developed perovskite–fluorite interfaces (Fig. 2).

3.2. Transport properties and reactivity

3.2.1. Conductivity

The total specific conductivity of nanocomposites mainly determined by the electronic conductivity of P phase usually increases with the sintering temperature due to porosity annealing and percolation improving [6–10]. It decreases with the content of electrolyte in nanocomposite (Fig. 3) both due to the effect of dilution with F phase possessing a lower specific conductivity as well as due to incorporation of Zr, Ce or Sc cations into the B sublattice of perovskite hampering jumps of electrons between

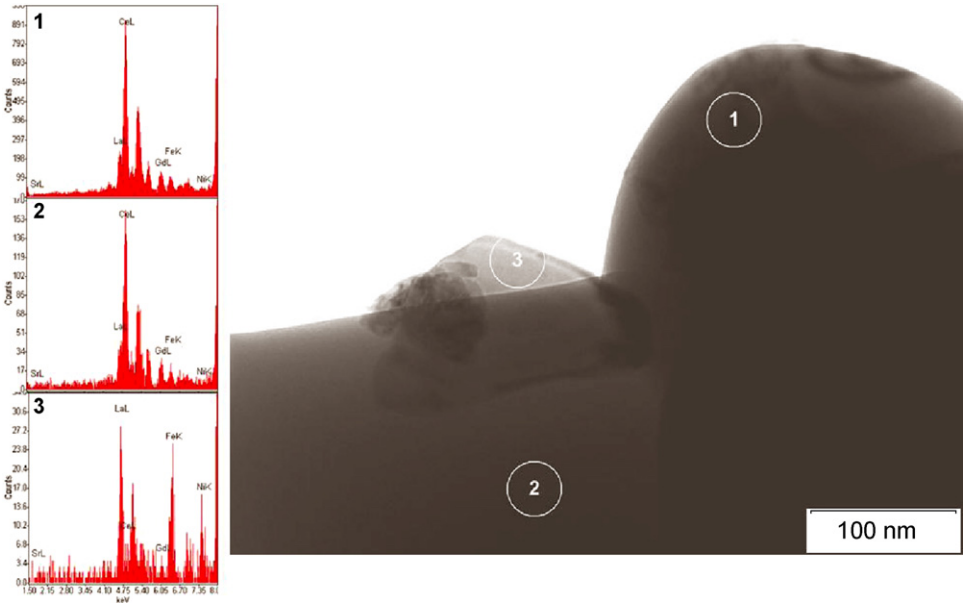

Fig. 1. Typical morphology of particles in LSNF–GDC composite sintered at 1200 °C and respective EDX spectra from regions 1 to 3. Elemental composition: (1) 19 wt.% $La_{0.97}Sr_{0.03}Fe_{0.68}Ni_{0.32}O_3$ + 81 wt.% $Ce_{0.93}Gd_{0.07}O_2$, (2) 21 wt.% $La_{0.94}Sr_{0.06}Fe_{0.74}Ni_{0.26}O_3$ + 79 wt.% $Ce_{0.93}Gd_{0.07}O_2$, (3) 82 wt.% $La_{0.98}Sr_{0.02}Fe_{0.63}Ni_{0.37}O_3$ + 18 wt.% $Ce_{0.68}Gd_{0.32}O_2$.

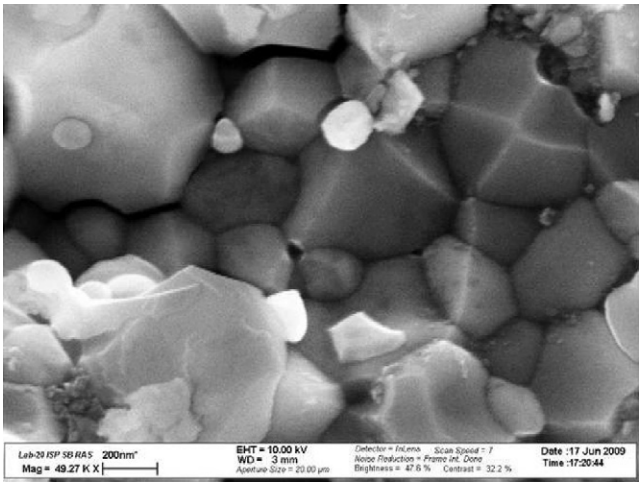

Fig. 2. SEM image of the cleaved surface of LSFN-GDC pellet sintered at 1200 °C.

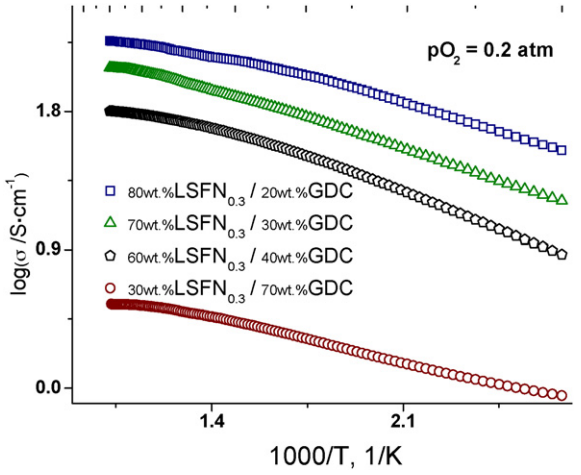

Fig. 3. Temperature dependence of conductivity for $La_{0.8}Sr_{0.2}Fe_{0.7}Ni_{0.3}O_{3-\delta}$–$Ce_{0.9}Gd_{0.1}O_{1.95}$ nanocomposites with different content of fluorite phase.

neighboring transition metal cations. Comparable values of total specific conductivity were also obtained for sintered LSM–ScCeSZ nanocomposites [6,8].

3.2.2. Oxygen isotope heteroexchange

Typical results of SSITKA experiments are shown in Fig. 4. For GDC and $LSFN_{0.3}$ samples, experimental data were fitted by a simple model of a uniform oxygen diffusion in the bulk, while for GDC–$LSFN_{0.3}$ nanocomposite satisfactory description was obtained only in the frames of a more complex model suggesting very fast oxygen exchange between the surface and perovskite–fluorite interfaces in the bulk of composite particles. This mobile oxygen is rapidly exchanged with GDC domains and slower – with LSFN domains. Bulk diffusion is the rate-limiting stage only for perovskite phase/domains, while for GDC phase/domains the rate of exchange is controlled by the surface reaction. Hence, for GDC only the lowest limit of the oxygen self-diffusion coefficient can be estimated.

Parameters of the oxygen diffusion estimated with a due regard for the typical sizes of perovskite and fluorite domains and amount of mobile oxygen atoms located at the perovskite–fluorite interfaces (less than ~2% of the overall oxygen amount in the sample, vide infra) are given in Table 1. Though more detailed analysis is required, the role of perovskite–fluorite interfaces as paths for fast oxygen diffusion in nanocomposites is demonstrated. Apparent activation energy of oxygen self-diffusion along perovskite–fluorite interfaces is ~110 kJ mol^{-1}, which is close to that in GDC [2].

For powdered samples of sintered LSM–ScCeSZ nanocomposites detailed studies of oxygen isotope heteroexchange in static

Table 1
Coefficients of oxygen self-diffusion in the fluorite phase D_F, perovskite phase D_P and along interfaces $D_{interface}$.

T (°C)	D_F ($cm^2\ s^{-1}$)	D_P ($cm^2\ s^{-1}$)	$D_{interface}$ ($cm^2\ s^{-1}$)
Nanocomposite			
600	$\geq 6 \times 10^{-14}$	2×10^{-14}	$\geq 1 \times 10^{-8}$
700	$\geq 30 \times 10^{-14}$	9×10^{-14}	$\geq 5 \times 10^{-8}$
Perovskite			
700		6×10^{-14}	$\geq 0.4 \times 10^{-8}$
Fluorite			
700	$>7 \times 10^{-14}$		$\geq 0.2 \times 10^{-8}$

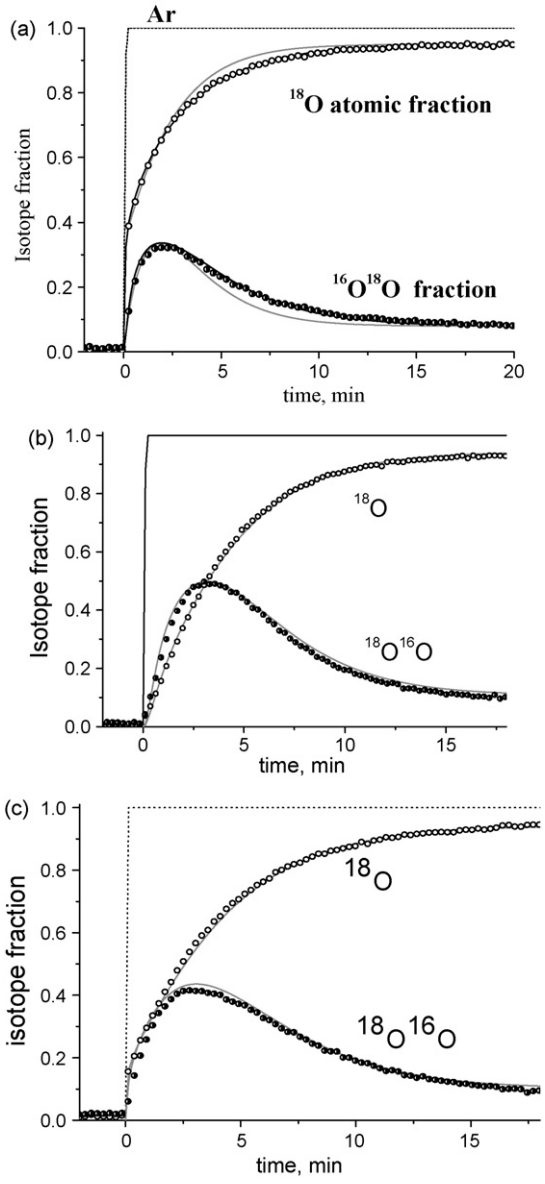

Fig. 4. Variation of ^{18}O and $^{16}O^{18}O$ fractions in the gas phase after switching the stream of 1% $^{16}O_2$ in He for the stream of 1% $^{18}O_2$ + 1%Ar in He at 700 °C. Points – experiment, gray line: fitting by the uniform diffusion model, black line: fitting by the heterogeneous diffusion model; (a) composite $La_{0.8}Sr_{0.2}Fe_{0.7}Ni_{0.3}O_{3-\delta}$–$Ce_{0.9}Gd_{0.1}O_{1.95}$, (b) perovskite $La_{0.8}Sr_{0.2}Fe_{0.7}Ni_{0.3}O_3$ and (c)fluorite $Ce_{0.9}Gd_{0.1}O_{1.95}$.

installation and temperature-programmed oxygen desorption revealed also a similar role of perovskite–fluorite interfaces as paths for fast oxygen diffusion [6,8].

3.2.3. Oxygen mobility and reactivity for dense samples

Both D_{chem} and k_{chem} estimated from the conductivity relaxation experiments tend to increase with GDC content in nanocomposite (Fig. 5), which agrees with conclusion on a high oxygen mobility along perovskite–fluorite interfaces based on results of SSITKA experiments for powdered samples (vide supra).

Similarly, the oxygen chemical diffusion coefficient estimated for dense nanocomposite samples from the weight loss dynamics data (Fig. 6) exceeds that for perovskite. This result also clearly demonstrates a positive role of perovskite–fluorite interfaces as paths for the fast oxygen transfer. The maximum value of the weight loss in these experiments corresponds to removal of

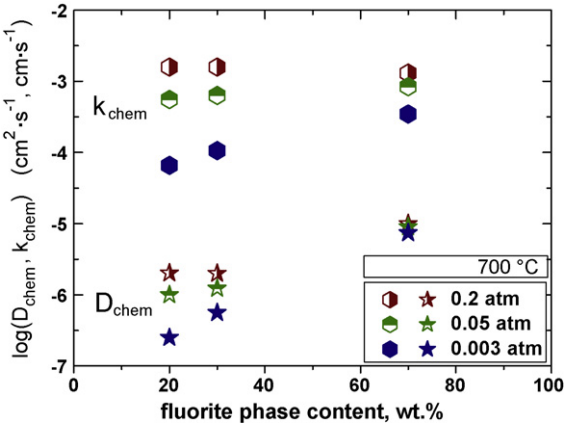

Fig. 5. Effect of fluorite phase content and oxygen partial pressure on D_{chem} and k_{chem} for $La_{0.8}Sr_{0.2}Fe_{0.7}Ni_{0.3}O_{3-\delta}$–$Ce_{0.9}Gd_{0.1}O_{1.95}$ nanocomposites.

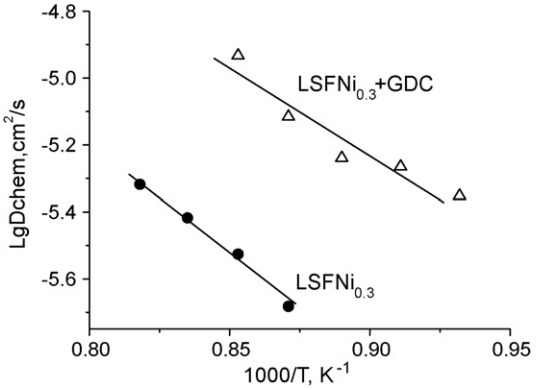

Fig. 6. Temperature dependence of D_{chem} for LSFN-GDC nanocomposite and LSFN perovskite.

less than 2% of the overall amount of oxygen atoms in composite. Apparent activation energy of the oxygen chemical diffusion (~110 kJ mol^{-1}) coincides with that of the oxygen self-diffusion along the perovskite–fluorite interfaces (vide supra). Hence, thus estimated oxygen chemical diffusion coefficient can indeed characterize the oxygen migration along the perovskite–fluorite interfaces in nanocomposite. The values of the oxygen chemical dif-

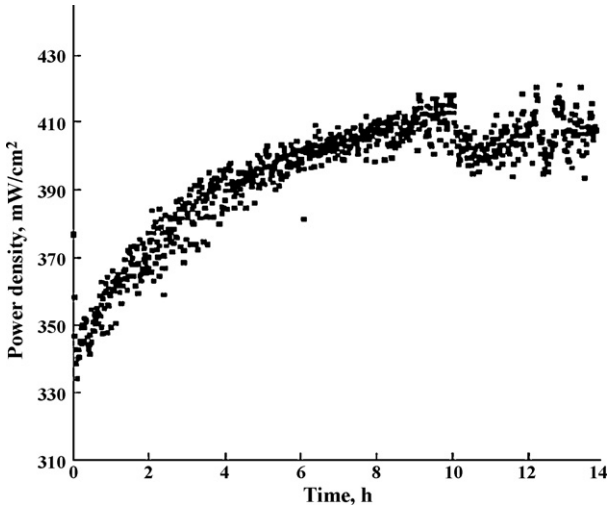

Fig. 7. Time dependence of the power density of the SOFC with the GDC functional layer between the LSFN cathode and the YSZ electrolyte under load of 0.5 V at 700 °C.

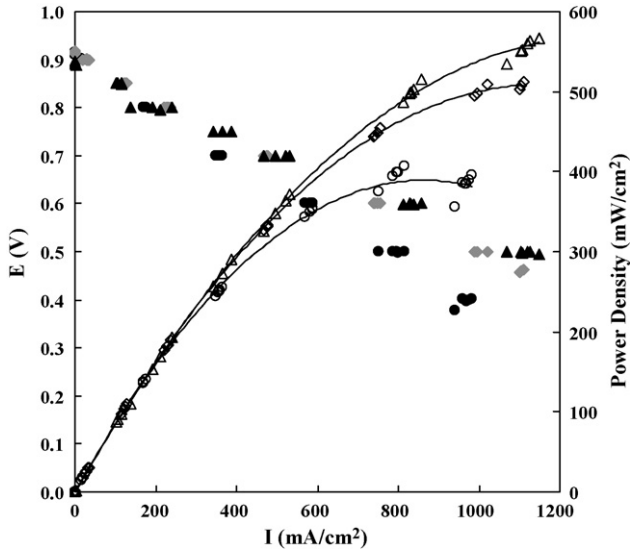

Fig. 8. Performance of the SOFC with the GDC functional layer between the LSFN cathode and YSZ electrolyte at different temperatures after 0.5 V load for 15 h at 700 °C. (●) – 700 °C; (♦) – 750 °C and (▲) – 800 °C.

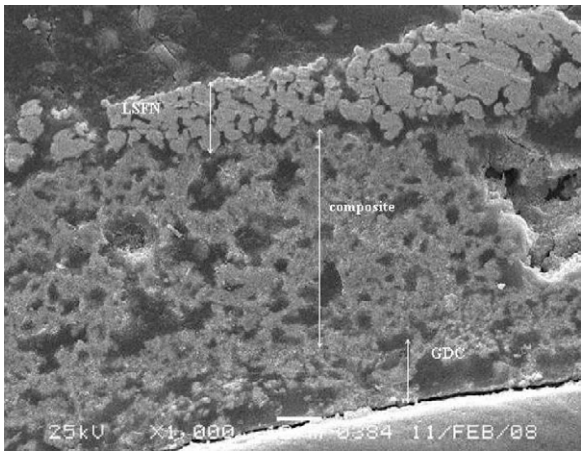

Fig. 9. SEM micrographs of a cell cross-section fragment near the cathode–electrolyte interface after testing SOFC with functionally graded cathode GDC/GDC + LSFN/LSFN.

fusion coefficient for GDC–$LSFN_{0.3}$ nanocomposite ($\sim 10^{-5}$ cm^2 s^{-1} at 1080 K) estimated by the weight loss and conductivity relaxation methods are close to those for the best single-phase MIEC $La_{0.6}Sr_{0.4}Co_{0.8}Fe_{0.2}O_{3-\delta}$ oxide [15].

3.3. Cell design and testing

3.3.1. Cells with GDC functional layer

For this type of design, despite sintering GDC interlayer at 1400 °C, it remained rather porous, so that subsequent supporting and sintering LSFN layer produced nanocomposite cathode with LSFN content increasing in direction electrolyte – air from 0 to 100%. Moreover, in this design the power density was increasing with time under load (Fig. 7), apparently, due to transfer of Ni^{2+} cations on the GDC and YSZ surface in slightly reducing conditions. As the result, performance in the intermediate temperature range was stable and promising for the practical application (Fig. 8).

Without GDC interlayer, the power density of cell with LSFN cathode was much lower not exceeding 60 mW cm^{-2} at 700 °C, which was shown to be due to formation of isolating La zirconate layer at LSNF–YSZ boundary [9]. In the case of GDC interlayer separating YSZ electrolyte and LSFN perovskite or its nanocomposite with GDC [9], such isolating zirconate layers were not observed after cell testing (Fig. 9).

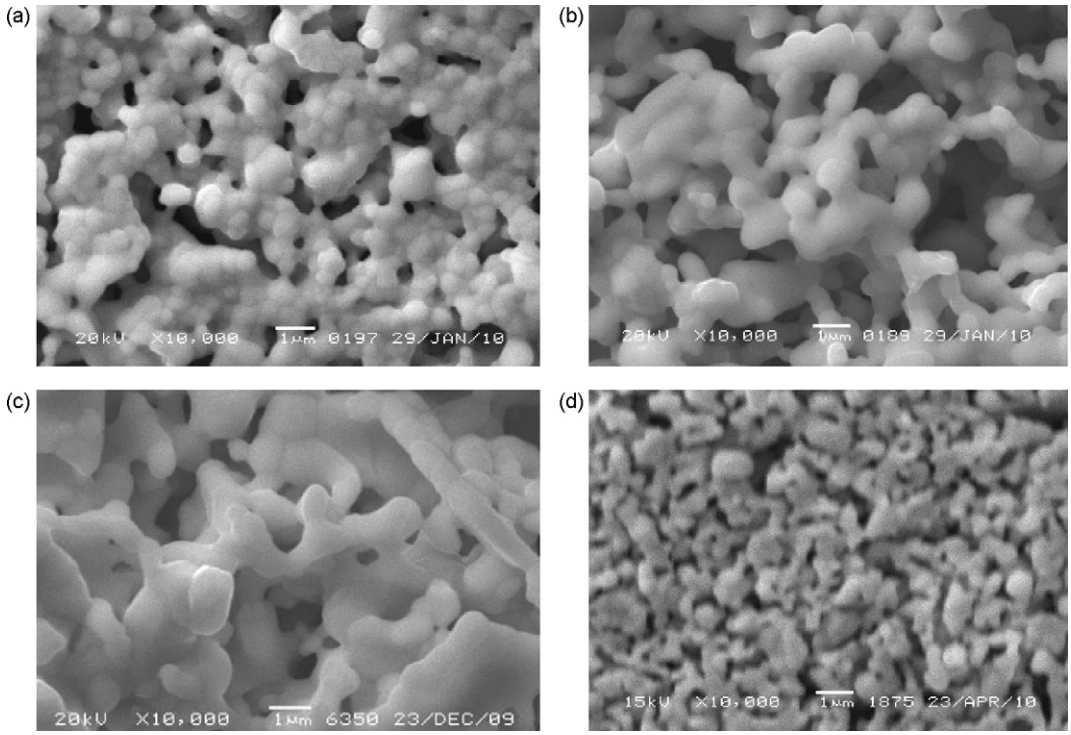

Fig. 10. Typical SEM images of nanocomposites interlayers supported on YSZ electrolyte and sintered in the furnace at 1200 °C (a and b), under e-beam (c) or microwave radiation (d). (a) LSFN–GDC nanocomposite sintered with Bi additive; (b) LSM–ScCeSZ nanocomposite sintered with Ag additive; (c) LSFN–GDC nanocomposite sintered under e-beam irradiation; (d) LSFN–GDC nanocomposite sintered under microwave irradiation.

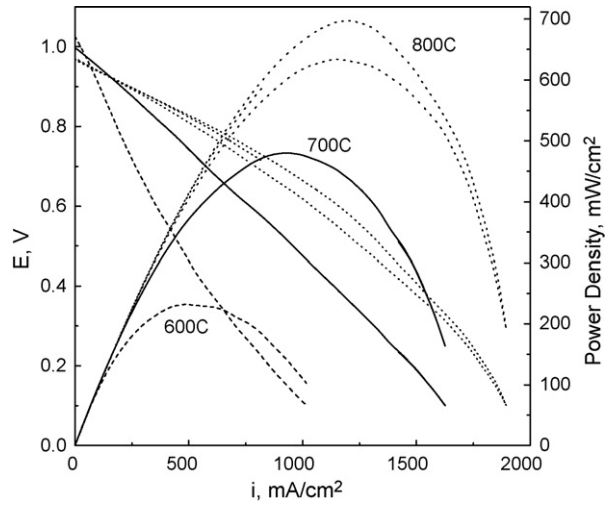

Fig. 11. Polarization and the power density curves for button-type cell with thin YSZ electrolyte, LSM–ScCeSZ nanocomposite interlayer sintered with Ag aid, LSNF cathode and Ag paste as a current collector.

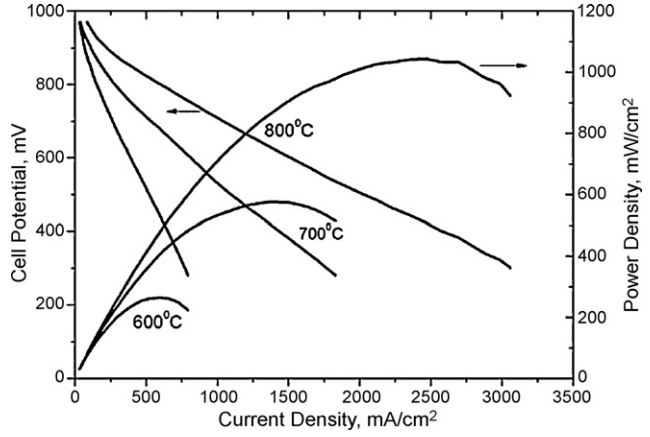

Fig. 12. Polarization and the power density curves for button-type cell on Ni-Al foam substrate supporting Ni/YSZ cermet layers, thin YSZ electrolyte, LSM–ScCeSZ interlayer sintered by e-beam action and LSM cathode.

3.3.2. Cells with thin nanocomposite interlayers

To optimize the thickness and microstructure of interlayers, nanocomposites were used instead of GDC because they in general sinter at lower temperatures and possess a higher oxygen mobility along perovskite–fluorite interfaces (vide supra). Typical images of nanocomposite interlayers sintered by using different approaches are shown in Fig. 10.

In general, the best results in terms of interlayer density were obtained with sintering under e-beam action, though sintering additives were also quite efficient. More specifically, Ag as a sintering aid is more efficient for LSM–ScCeSZ nanocomposite, while Bi for this system is not efficient at all, perhaps, due to its easy incorporation into the manganite lattice. Microwave irradiation also provides better results than the usual thermal sintering, though its combination with sintering aids could also be promising.

The maximum power density of cells with thin and rather dense nanocomposite interlayers (Figs. 11 and 12) is higher than that for the cell with rather loose GDC interlayers (Fig. 8), which apparently can be explained by a high lattice oxygen mobility along perovskite–fluorite interfaces. In this respect, the lattice oxygen mobility in a porous perovskite layer covering nanocomposite interlayer is clearly less important, since for LSM (Fig. 12) with a low lattice oxygen mobility performance is even better than for LSFN with a high lattice oxygen mobility. Cell performance was stable under load for at least 20–50 h. SEM studies of discharged cells cross-sections have not revealed any traces of isolating zirconate layers between YSZ electrolyte and nanocomposite interlayers [16].

4. Conclusions

Perovskite–fluorite nanocomposites (LSFN-GDC, LSM–ScCeSZ) prepared by powerful ultrasonic treatment of the mixture of nanocrystalline oxides in isopropanol with addition of polyvinyl butyral demonstrate enhanced oxygen mobility due to fast oxygen transfer along perovskite–fluorite interface. Nanocomposite perovskite–fluorite interlayers of optimized composition and sintered at temperatures not exceeding 1200 °C using sintering aids or radiation–thermal treatment provide high and stable performance of cells with thin YSZ layers and perovskite LSM or LSFN cathodes due to their high lattice oxygen mobility and suppression of Zr migration endangering isolating zirconate layers formation.

Acknowledgements

The authors gratefully acknowledge the financial support from NATO SFP 980878, SOFC 600 FP6 EC Project, Integration Project 57 of CB RAS-NAN Belarus, Project 57 of RAS Presidium Program No. 27 and RFBR-ofi_m 09-03-12317 Project.

References

[1] M. Rieu, R. Sayers, M.A. Laguna-Bercero, S.J. Skinner, P. Lenormand, F. Ansart, Electrochem. Soc. Trans. 25 (2009) 2565–2571.
[2] A. Esquirol, J. Kilner, N. Brandon, Solid State Ionics 175 (2004) 63–67.
[3] F. Zhao, X. Wang, Zh. Wang, R. Peng, Ch. Xia, Solid State Ionics 179 (2008) 1450–1453.
[4] H.-G. Jung, Y.-K. Sun, H.Y. Jung, J.S. Park, H.-R. Kim, G.-H. Kim, H.-W. Lee, J.-H. Lee, Solid State Ionics 179 (2008) 1535–1539.
[5] S. Bebelis, N. Kotsionopoulos, A. Mai, D. Rutenbeck, F. Tietz, Solid State Ionics 177 (2006) 1843–1848.
[6] V. Sadykov, S. Pavlova, V. Zarubina, A. Bobin, G. Alikina, A. Lukashevich, V. Muzykantov, V. Usoltsev, T. Kharlamova, A. Boronin, S. Koscheev, T. Krieger, A. Ishchenko, N. Mezentseva, A. Salanov, A. Smirnova, O. Bobrenok, N. Uvarov, Electrochem. Soc. Trans. 25 (2009) 2403–2412.
[7] V. Sadykov, T. Kharlamova, L. Batuev, N. Mezentseva, G. Alikina, V. Muzykantov, T. Krieger, S. Pavlova, V. Zaikovskii, A. Ishchenko, V. Zarubina, V. Rogov, O. Bobrenok, N. Uvarov, J. Kilner, J. Druce, A. Smirnova, Mater. Res. Soc. Symp. Proc. 1098 (2008) 1–6, 1098-HH07-06.
[8] V. Sadykov, V. Muzykantov, A. Bobin, L. Batuev, G. Alikina, A. Lukashevich, A. Boronin, T. Krieger, A. Ishchenko, O. Bobrenok, N. Uvarov, A. Smirnova, O. Vasylyev, Mater. Res. Soc. Symp. Proc. 1126 (2009) 1–6, S13-03.
[9] T. Kharlamova, A. Smirnova, V. Sadykov, V. Zarubina, T. Krieger, L. Batuev, A. Ishchenko, A. Salanov, N. Uvarov, Electrochem. Soc. Trans. 13 (2008) 275–284.
[10] V. Sadykov, T. Kharlamova, L. Batuev, V. Muzykantov, N. Mezentseva, T. Krieger, G. Alikina, A. Lukashevich, V. Rogov, V. Zaikovskii, A. Ishchenko, A. Salanov, A. Boronin, S. Koscheev, S. Pavlova, N. Uvarov, A. Smirnova, O. Vasylyev, Compos. Interfaces 16 (2009) 407–431.
[11] E.M. Sadovskaya, Y.A. Ivanova, L.G. Pinaeva, G. Grasso, T.G. Kuznetsova, A. van Veen, V.A. Sadykov, C. Mirodatos, J. Phys. Chem. A 111 (2007) 4498–4505.
[12] J. Crank, The Mathematics of Diffusion, Oxford University Press/J.W. Arrowsmith LTD., Bristol, 1975.
[13] B. Ma, U. Balachandran, J.-H. Park, C.U. Segre, Solid State Ionics 83 (1996) 65–71.
[14] J.A. Lane, J.A. Kilner, Solid State Ionics 136/137 (2000) 997–1001.
[15] M. Katsuki, Sh. Wang, M. Dokiya, T. Hashimoto, Solid State Ionics 156 (2003) 453–461.
[16] A. Smirnova, V. Sadykov, N. Mezentseva, V. Usoltsev, O. Smorygo, O. Bobrenok, N. Uvarov, in: Proceedings of the 8th International Fuel Cell Science, Engineering and Technology Conference, FuelCell2010, June 14–16, Brooklyn, New York, USA (2010), paper 33268.